XII. PHYSICAL ELECTRONICS AND SURFACE PHYSICS

A. Surface Physics*

Academic and Research Staff

Prof. R. E. Stickney
Dr. M. L. Shaw

Graduate Students

J. W. Gadzuk
R. M. Logan
D. S. Shupe

RESEARCH OBJECTIVES

The general purpose of this research program is to study the interaction of gas molecules with solid surfaces. At present, we are concerned with four principal problems.

1. Adsorption

During the past year we developed a quantum-mechanical treatment of the adsorption of alkali-metal atoms on metallic surfaces (see Sec. XII-A. 1). We are now preparing to perform experiments designed to test the validity of the theoretical model and analytical solutions.

2. Gas-Surface Conditions

Using a simple classical model, we have successfully described the general features of the scattering of gas molecules from solid surfaces (see Quarterly Progress Report No. 79, pages 67-71). This analysis will continue, and a quantum-mechanical treatment will be attempted. We are also planning an experimental investigation of the scattering of molecular beams from solid surfaces.

3. Catalysis

An ultrahigh vacuum system suitable for studies of catalysis has been completed. Using a mass spectrometer, we shall measure the gaseous products of chemical reactions occurring on the surfaces of various materials. We plan first to consider the catalytical formation of ammonia.

4. Photoinduced Surface Processes

Our experimental investigation of the effects of thermal and ultraviolet light on the thermionic emission from tungsten has been completed (see Sec. XII-A. 3), and we are now attempting to extend the study to cesium-covered tungsten.

R. E. Stickney

1. VALENCE-LEVEL SHIFT OF AN ALKALI ATOM AS A RESULT OF INTERACTING WITH A METAL SURFACE

If an alkali atom is allowed to interact with a metal at the surface of the metal, as shown in Fig. XII-1, the valence level of the alkali which we call the ns level (n is the

*This work is supported by the Joint Services Electronics Programs (U.S. Army, U.S. Navy, and U.S. Air Force) under Contract DA 36-039-AMC-03200(E).

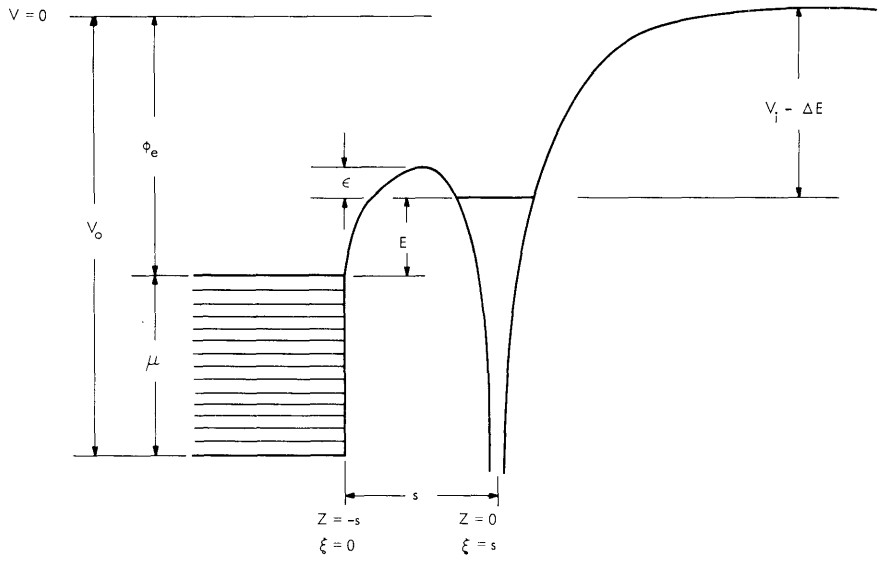

Fig. XII-1. Model for the atom-metal interaction.

principal quantum number) will be shifted from its unperturbed energy. The shifted level will also broaden. A theoretical approach to the natural width has been previously reported.[1] In the present report, the position of the band center of the perturbed alkali atom is calculated.

Theory

If the Hartree-Fock equations for the metal-alkali system are interpreted correctly, it can be shown[2] that the interaction between the ns electron and the metal perturbed by the alkali ion core is

$$H' = \frac{q^2}{R} - \frac{q^2}{4d_1} \qquad (1)$$

in which R is the distance between the ns electron and the image charge of the alkali ion core, and d_1 is the distance between the ns electron and the surface. This is readily understood from the classical point of view, as shown in Fig. XII-2.

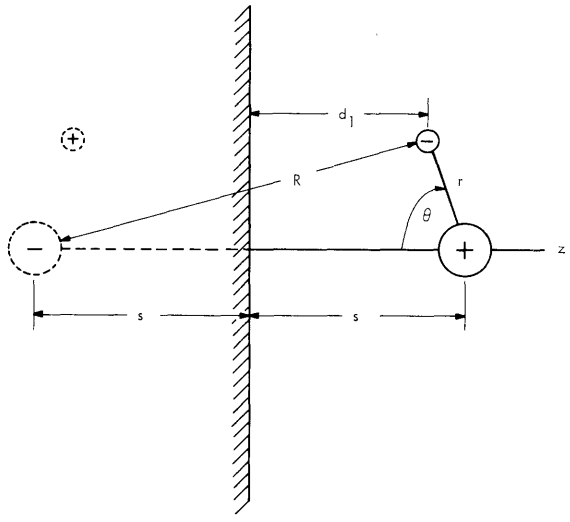

Fig. XII-2. Classical picture of the atom and the image charges that it induces in the metal.

As the alkali atom is allowed to interact with a metal through the interaction given by Eq. 1, the first-order energy

shift is given by

$$\Delta E = \frac{\langle ns|\mathcal{H}'|ns\rangle}{\langle ns|ns\rangle} . \tag{2}$$

The coordinate system used in the calculations of the energy shift is one with the origin, z = 0, at the center of the ion core and with z increasing positively away from the metal. In this system, shown in Fig. XII-2, the distance of the electron from the metal surface is given by $d_1 = s - |r\cos\theta| = s - |z|$. The distance between the electron and the ion core image is given by $R \approx 2s - |r\cos\theta| = 2s - |z|$. This is a very good approximation for small r, which is the only region in which the electron charge density is significant. The unperturbed ns wave functions are taken to be fitted hydrogen 2s wave functions as described previously.[1] With hydrogenic wave functions and Eq. 1, Eq. 2 becomes

$$\Delta E = \frac{\displaystyle\int_0^{s-s_c} dz \left(\frac{q^2}{2s-|z|} - \frac{q^2}{4(s-|z|)}\right)\left\{\iint_{-\infty}^{+\infty} dxdy\,(1-2ar+a^2r^2)\,e^{-2ar}\right\}}{\displaystyle\int_0^{s-s_c} dz \left\{\iint_{-\infty}^{+\infty} dxdy\,(1-2ar+a^2r^2)\,e^{-2ar}\right\}}, \tag{3}$$

where the integration has been restricted to the region outside the metal. The value of s_c is chosen so that the integration stops when the image potential reaches that which exists at the bottom of the conduction band. Mathematical details of the integration will appear elsewhere,[2] so only the end result is given here in an extremely cumbersome, but exact, closed form. It is found that

$$\begin{aligned}\Delta E = 1.8a\Big\{&-30a^2s^2 - \tfrac{9}{2} + 4e^{-4as}(32a^3s^3-8a^2s^2+4as+1)\int_{2as}^{4as} dt\,\frac{e^t}{t} + e^{-2as}(4a^3s^3\\ &-2a^2s^2+2as+1)\int_{2as_c}^{2as} dt\,\frac{e^t}{t} - e^{-2a(s-s_c)}\left(2a^2s_c^2-as_c+\tfrac{3}{2}+6a^2s^2+3as-6a^2s_cs\right)\\ &+e^{-2as}(56a^2s^2+4as+6)\Big\}\Big/\left\{2-e^{-2as}\left(a^3s^3+a^2s^2+\tfrac{3}{2}as+1\right)\right\},\end{aligned} \tag{4}$$

where ΔE is given in electron volts, s in angstroms, and a, which is a characteristic of the particular alkali in question, in inverse angstroms. Numerical values for the exponential integral are tabulated as a function of the upper limit.[3] Equation 4 is evaluated as a function of distance from the surface for the specific cases of potassium on platinum and cesium on tungsten and the graph of this function appears in Fig. XII-3.

Note that both curves exhibit the shape suggested by Gomer[4, 5] at distances greater than approximately the sum of one-half the lattice constant plus the alkali ionic radii ≈3 - 4 Å.

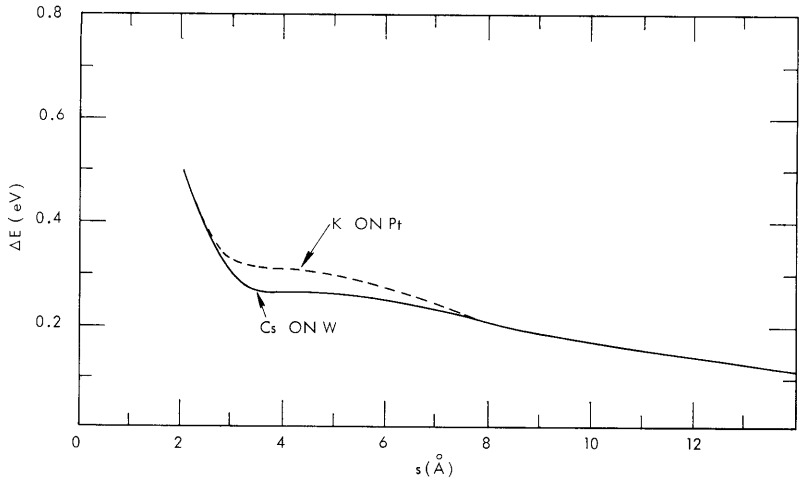

Fig. XII-3. Energy-level shift determined from Eq. 2 as a function of atom-metal separation for cesium-tungsten and potassium-platinum.

This is the atom-metal separation when the atom becomes adsorbed. The results are not really meaningful at smaller separations, as these separations would physically be prohibited by other repulsive forces not included in this formalism. Note that the energy level has been shifted upward in both cases by approximately 0.3 ev for an adsorbed alkali. This is in accord with the value of 0.35 ev suggested by Rasor[6] and Levine.[7]

The relevance of this calculation to theories of adsorption is discussed in a paper that has been submitted to the Journal of Chemical Physics.[2]

J. W. Gadzuk

References

1. J. W. Gadzuk, "Bonding Mechanism of Alkali-Metal Atoms Adsorbed on Metal Surfaces," Quarterly Progress Report No. 77, Research Laboratory of Electronics, M.I.T., April 15, 1965, pp. 238-244.
2. J. W. Gadzuk, "Theory of Metal-Alkali Atom Interactions" (submitted to J. Chem. Phys.).
3. E. Jahnke and F. Ende, "Tables of Functions" (Dover Publications, Inc., New York, reprint 1945).
4. R. Gomer and L. W. Swanson, J. Chem. Phys. 38, 1613 (1963).
5. L. Schmidt and R. Gomer, J. Chem. Phys. 42, 3573 (1965).
6. N. S. Rasor and C. Warner III, J. Appl. Phys. 35, 2589 (1964).
7. J. D. Levine and E. P. Gyftopoulos, Surf. Sci. 1, 171; 225; 349 (1964).

2. INDUCED AND SPONTANEOUS TRANSITIONS IN GAS-SURFACE INTERACTIONS

The problem of energy exchange in the interaction of a monatomic gas with a solid surface is considered by using the concept of induced and spontaneous transitions and the principle of detailed balancing. The problem is treated as the interaction of a gas atom with the phonons of the solid. The first part of the analysis is analogous to the well-known analysis[1] of the interaction of an atom (or molecule) with the photons of a radiation field.

Consider some gas atoms in an enclosure, in which the gas density is so low that collisions between the atoms are very infrequent compared with collisions with the surface. Define the following quantities:

$p_{ij}dt$ = the probability that a gas atom in state i (kinetic energy E_i) will undergo transition to state j in time dt.

R_{ij} = the probability that a gas atom incident upon the surface in state i will leave the surface in state j.

γ_i = the average number of collisions with the surface per unit time for a particular gas atom in state i.

From these definitions it follows that $R_{ij} = P_{ij}/\gamma_i$. By analogy with the analysis for electromagnetic radiation,[1] the transition of the gas atom between states with kinetic energies E_i and E_j ($E_i > E_j$) is described by the following expressions.

$$P_{ij} = A_{ij} + U(\nu, T_s)\, B_{ij} \tag{1}$$

$$P_{ji} = U(\nu, T_s)\, B_{ji}, \tag{2}$$

where

A_{ij} = the coefficient for spontaneous transition,

B_{ij} = the coefficient for induced transition,

$U(\nu, T_s)$ = phonon energy density per unit frequency range in the solid at temperature T_s.

The assumptions about the transitions as expressed by Eqs. 1 and 2, together with the following analysis, are only reasonable for single phonon transitions.

a. Equilibrium Situation

Consider a gas in equilibrium with the enclosure at temperature T_s. Let the number of atoms in states i and j at equilibrium be N_i and N_j, respectively. Let the degeneracies of the energy states i and j be D_i and D_j, respectively. From the principle of detailed balancing it follows that, at equilibrium, $N_i P_{ij} = N_j P_{ji}$. For the phonon field assume a relation of the usual form,[2]

$$U(\nu, T_s) = G(\nu)/[\exp(h\nu/kT_s)-1],$$

where $G(\nu)$ is a function of ν and of the properties of the solid, but not of T_s.

By proceeding as in the photon problem,[1] relations can be obtained among the A_{ij}, B_{ij}, and B_{ji}. By using these relations in Eqs. 1 and 2, we obtain

$$R_{ij} = \frac{A_{ij} + U(\nu_{ij}, T_s)\, B_{ij}}{\gamma_i} = \frac{A_{ij}}{\gamma_i}\left[\frac{1}{1 - \exp(-h\nu_{ij}/kT_s)}\right] \tag{3}$$

$$R_{ji} = \frac{U(\nu_{ij}, T_s)\, B_{ji}}{\gamma_j} = \frac{A_{ij}}{\gamma_j}\frac{D_i}{D_j}\left[\frac{1}{\exp(h\nu_{ij}/kT_s) - 1}\right], \tag{4}$$

where $h\nu_{ij} = E_i - E_j$. Although they have been derived for the equilibrium situation, these expressions for R_{ij} and R_{ji} may now be applied to the collision of a gas atom with the surface, irrespective of whether the gas is in equilibrium with the surface. The additional restriction of low gas density may also be dropped.

b. Gas with Equilibrium Distribution at Temperature T_g

Assume that the gas has an equilibrium distribution at temperature T_g, with $T_g \neq T_s$. This situation, of a surface at temperature T_s in the presence of a gas at temperature T_g ($T_g \neq T_s$), actually occurs in the usual experimental arrangement for measuring energy accommodation coefficients.[3] Let ξ_i be the number of atoms in state i striking the surface per unit area per unit time.

The expectation value of the net energy exchange, associated with the energy levels i and j, from the surface to the gas per unit area per unit time is given by

$$\epsilon_{ij} = h\nu_{ij}(\xi_j R_{ji} - \xi_i R_{ij}). \tag{5}$$

From the definition of γ_i it follows that $\xi_i/\gamma_i = N_i/K$, where K is some factor that depends upon the geometry of the surface and will be constant for a given gas-surface system. For a Maxwellian distribution at temperature T_g, $(N_j D_i/N_i D_j) = \exp(\sigma_g)$, where $\sigma_g = h\nu_{ij}/kT_g$. From Eqs. 3, 4, and 5 we then obtain

$$\epsilon_{ij} = C_{ij}\left[\frac{e^{\sigma_s}}{e^{\sigma_g} - 1} - \frac{1}{1 - e^{-\sigma_s}}\right] \tag{6}$$

where $\sigma_s = h\nu_{ij}/kT_s$, and $C_{ij} = h\nu_{ij} K N_i A_{ij}$ is constant for a given gas-surface system and a given pair of energy levels, i and j.

The terms in Eq. 6 can be written as infinite series, and if we assume that σ_s and σ_g are of order 1, or less, and neglect small terms, Eq. 6 becomes

$$\epsilon_{ij} \approx C_{ij}\left[1 + \frac{\sigma_g}{2} + \frac{\sigma_g^2}{6} - \frac{\sigma_g^2}{12}\left(\frac{T_g}{T_s}\right) + \frac{\sigma_g^3}{24} - \frac{\sigma_g^3}{24}\left(\frac{T_g}{T_s}\right)\right](T_s - T_g)/T_g. \tag{7}$$

If σ_g is of magnitude 1, or less, and $T_s > T_g$, it is reasonable to neglect the terms involving (T_g/T_s) in Eq. 7. Hence,

$$\epsilon_{ij} \approx C_{ij}\left(1 + \frac{\sigma_g}{2} + \frac{\sigma_g^2}{6} + \frac{\sigma_g^3}{24}\right)(T_s - T_g)/T_g. \tag{8}$$

If we put $h\nu_{ij} = \beta k\theta$, where θ is the Debye temperature, then $\sigma_g = \beta\theta/T_g$; $h\nu_{ij}$ is the energy of one phonon and $k\theta$ is, approximately, the maximum energy that a phonon may have. Thus β is a positive number less than 1, and a sufficient, but not necessary, condition for $\sigma_g < 1$ is $T_g \geq \theta$. From Eq. 7 it is seen that the condition $\sigma_g \lesssim 1$ may be relaxed as the ratio T_s/T_g increases.

c. Conclusions

The over-all net energy exchange from the surface to the gas is obtained by summing over all pairs of states ij in Eq. 6. It follows from Eq. 8 that, when T_g is constant, this energy exchange is approximately proportional to $(T_s - T_g)$. The energy accommodation coefficient is given by

$$\alpha = \frac{\text{net energy exchange to gas}}{2k(T_s - T_g)}. \tag{9}$$

Upon substituting for the net energy exchange in Eq. 9 the factor $(T_s - T_g)$ cancels, and thus the analysis predicts that α is approximately constant as T_s is varied (for $T_s > T_g$ and T_g constant). This result agrees with the experimental results of Thomas and Schofield[3] and Moreton[4] for helium and neon on tungsten and platinum surfaces.

R. M. Logan

References

1. For example, N. Davidson, Statistical Mechanics (McGraw-Hill Series in Advanced Chemistry, New York, 1962), p. 222.
2. See, for example, F. Seitz, Modern Theory of Solids (McGraw-Hill Publishing Company, New York, 1940), p. 102.
3. L. B. Thomas and E. B. Schofield, J. Chem. Phys. 23, 861 (1955).
4. W. Watt and R. Moreton, Technical Note CPM 80, R.A.E., Farnborough, England, 1964.

3. EFFECT OF THERMAL AND ULTRAVIOLET RADIATION ON THERMIONIC EMISSION FROM TUNGSTEN

a. Introduction

Our interest in the effects of thermal and ultraviolet radiation on electron emission from metals at high temperatures was stimulated by the results of a simple experiment performed by A. Shavit, a member of our laboratory. Shavit found that the emission from a hot tungsten cathode in a low-pressure cesium diode increases significantly when radiation from the sun is focused upon the cathode. Hoping that this effect was an anomalous high-temperature photoelectric effect that might be used to enhance the performance of thermionic energy converters, we initiated the present investigation in which cesium vapor was not introduced into the diode because its presence complicates attempts to interpret the data.

From the experimental data reported here, we conclude that, rather than being the result of a photoelectric process, the emission enhancement may be explained simply as an increase in the thermionic emission caused by radiant heating of the cathode. In effect, the diode acts as a transducer that produces a measurable electrical output signal for radiation inputs of rather low intensity. Hence the thermionic diode may be used as a radiation detector. This application, and others, will be discussed briefly following the description of the experimental procedure and results.

A detailed discussion of the results has been omitted, since this may be found in a paper by the present authors which has been submitted for publication to the Journal of Applied Physics.

b. Experimental Apparatus

The experimental diode and circuitry are shown schematically in Fig. XII-4. The cathode, a $4.5 \times 0.32 \times 0.0025$ cm polycrystalline tungsten ribbon, is heated resistively. The collector is a rectangular tantalum box having a 0.32×3.2 cm slit in the front face to allow radiation to impinge upon the cathode. A magnetically operated shutter is provided to cover the quartz window during the high-temperature aging of the cathode. An ionization gauge and a titanium getter are attached to the diode.

The diode is evacuated by a two-stage mercury diffusion pump through a trap that is cooled by liquid hydrogen. After several bakeout and outgassing cycles, the titanium getter is flashed and the diode then sealed off from the vacuum system. The pressure remains in the 10^{-9}-torr range throughout the experiments. We believe that the cathode surface is both clean and stable because it has been aged thoroughly at 2400°K, emission measurements are reproducible and stable over long time intervals, and the diode pressure does not rise above the 10^{-9}-torr range when the cathode temperature is increased to 2400°K.

The Richardson equation[1] for thermionic emission from a metallic surface of area S at uniform temperature T is

$$I = SAT^2 e^{-\phi/kT}, \qquad (1)$$

where A and ϕ may depend upon the temperature and the nonuniformity of the surface work function. Our experimental data taken for a temperature range 1360°K < T < 2000°K can be fitted by Eq. 1 with

$$SA = 400 \frac{\text{amps}}{(^\circ K)^2} \quad \text{and} \quad \phi = 4.6 \text{ ev.}$$

A work function of 4.6 ev is reasonable for clean tungsten.

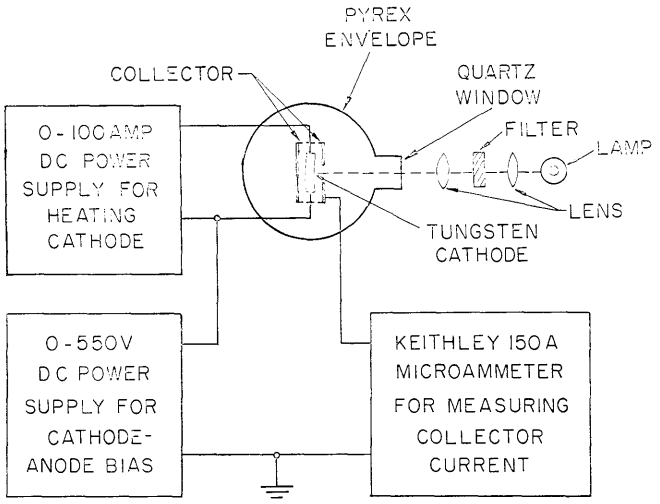

Fig. XII-4. Diagram of diode and associated optical and electrical components.

Quartz lenses are used to focus the radiation from a high-pressure mercury lamp (Bausch and Lomb HP-100) upon the cathode. In order to obtain high radiation intensity at the cathode, Corning sharp-cut filters are employed instead of a monochromator. The radiation intensity at the cathode for each filter is measured with a calibrated thermopile placed at the position normally occupied by the diode.

c. Experimental Procedure and Results

After attaining the desired cathode temperature by setting the heating power at the appropriate value, the cathode-anode voltage is increased until the thermionic current saturates. With the cathode completely shielded from the lamp radiation, the zero-suppress circuit in the Keithley 150A microammeter is adjusted to cancel the thermionic current. (In some cases, we have used a homemade circuit to supplement the zero-suppress capabilities of the meter.) The radiation shield is then removed and the current resulting from unfiltered radiation is recorded. Following this, filter 9-30 is placed in the radiation path and the current is recorded. Next, filter 9-30 is replaced by filter 0-54 and the current is recorded. This procedure is repeated for each of the filters.

By subtracting the emission currents associated with two different filters, we obtain the current resulting from the radiation band between the two filters. For example, if I_1 and I_2 are the currents measured for filters 9-30 and 0-54, then $\Delta I = I_1 - I_2$ is the current produced primarily by radiation associated with the 3100 Å line, which is the

Table XII-1. Radiation bands isolated by filter pairs.

Filter	Radiation Intensity Q (mw/cm^2)	ΔQ (mw/cm^2)	Wavelength Limits (Å)	Photon Energy Limits (ev)	Approximate Principal Wavelength in Band (Å)
None	12.6	2.80	$\lambda \leq 2500$	$h\nu > 4.96$	Many lines in far ultraviolet
9-30	9.8	1.60	2500-3200	4.96-3.88	3100
0-54	8.20	1.26	3200-3700	3.88-3.36	3640
0-51	5.94	0.64	3700-4200	3.36-2.96	4050
3-73	5.30	0.75	4200-4700	2.96-2.64	4350
3-71	4.55	0.95	4700-5600	2.64-2.22	5460
3-67	3.60	0.88	5600-5900	2.22-2.10	2780 (2 lines)
2-63	2.72				

brightest line emitted by the lamp in the band $2500 \lesssim \lambda \lesssim 3200$ isolated by these two filters (see Table XII-1). The filters have been selected to separate the more intense lines in the lamp spectrum so that, although each pair of filters isolates, at best, a band of radiation, one line or closely spaced set of lines will predominate. (This technique is perhaps less satisfactory in the ultraviolet where there are many closely spaced nearly equally intense lines, but it seems to be adequate for the purposes of our investigation.) The experimental results shown in Fig. XII-5 are described in terms of Γ, the emission current per unit radiation intensity,

$$\Gamma = \frac{\Delta I}{\Delta Q}, \tag{2}$$

where $\Delta Q = Q_1 - Q_2$ is the radiation intensity of the band between the filters, Q_1 and Q_2 being the intensities measured for each of the filters. The values of Q and ΔQ are recorded in Table XII-1, together with the approximate wavelengths (λ) and photon energies ($h\nu$) of the radiation bands associated with each pair of filters.

d. Concluding Remark

A detailed discussion of the feasibility of employing the thermionic diode as a radiation detector has been presented by R. C. Jones.[2] He concludes that although no

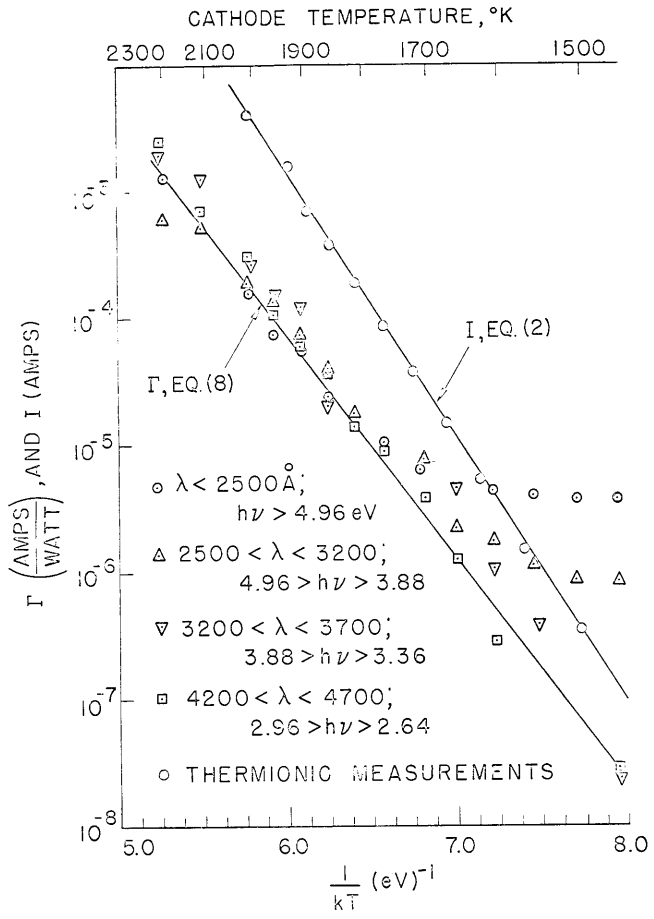

Fig. XII-5. Dependence of radiation-induced thermionic emission, Γ, on cathode temperature and radiation wavelength. The total thermionic emission current, I, is also included for comparison. Notice that the photoelectric current is predominant when $\lambda < 3200$ Å and $T < 1600°K$.

experimental data are available, this technique merits further investigation.

We have performed additional experiments which demonstrate that a thermionic diode may be used to determine the dependence of emissivity on radiation wavelength for materials at very high temperatures. There are other possible uses if atoms instead of photons are allowed to impinge upon the cathode. For example, it may be possible to measure energy accommodation coefficients and the probabilities of dissociation or recombination at hot surfaces. This technqiue might also be used as a detector of high-speed or highly excited molecular beams.

The effect of radiation on the thermionic characteristics of a diode may present problems in certain experiments. For example, measurements of photoelectric emission at moderate cathode temperatures will be obscured by increases in the thermionic emission

unless the cathode is so massive that the radiation produces a negligible change in the temperature. It is also possible that radiation and reflection from the anode or enclosure may introduce errors into measurements of the thermionic properties of materials.

R. A. Stickney, P. B. Sun, M. L. Shaw

References

1. C. Herring and M. H. Nichols, Rev. Modern Phys. 21, 185 (1949).
2. R. C. Jones, Advances in Electronics, Vol. V, edited by L. Marton (Academic Press, Inc., New York, 1953), p. 2.

XII. PHYSICAL ELECTRONICS AND SURFACE PHYSICS

B. Surface Properties of Thermionic Electrodes*

Academic and Research Staff

Prof. R. E. Stickney
J. G. Bergman

Graduate Students

W. Engelmaier
D. L. Fehrs

RESEARCH OBJECTIVES

The general objective of this program is to determine the surface properties of electrodes which are particularly relevant to thermionic energy conversion. A more specific objective is to obtain both experimental and analytical data on the dependence of work function on cesium coverage, surface contamination, and substrate properties (e.g., bare work function, crystallographic structure and temperature).

R. E. Stickney

*This work is supported by the National Aeronautics and Space Administration (Grant NGR-22-099-091).

XII. PHYSICAL ELECTRONICS AND SURFACE PHYSICS

C. Free-Molecule Flow Fields*

Academic and Research Staff

Prof. R. E. Stickney

Graduate Students

Y. S. Lou
S. Yamamoto

RESEARCH OBJECTIVES

In this program we are investigating the flow of gases in the transition regime between the free-molecule and continuum limits. Of primary interest is the near free-molecule flow regime for orifices and tubes exhausting into a vacuum. During the past year, we have obtained measurements of the angular distribution of the flow intensity as a function of the upstream pressure (see Sec. XII-C. 1). At present, we are modifying the apparatus so that velocity distribution measurements may be performed. Analytical treatments of the problem will also continue to be considered.

R. E. Stickney

1. ANGULAR DISTRIBUTION OF ORIFICES AND TUBES AT HIGH KNUDSEN NUMBERS

The angular distributions of flow from orifices and cylindrical tubes have been determined experimentally for Knudsen numbers of ~1 to 100. (The Knudsen number is defined here as the ratio λ/D, where λ is the mean-free path, and D is the diameter of the orifice or tube.) These results are summarized here. A detailed description of the apparatus and the results may be found in the theses of Hastings[1] and Keating.[2]

Orifice Flow

The experimental apparatus is designed so that we may measure I, the intensity of the flow downstream of the orifice, as a function of ϕ, the angular position from the center line. In the limit of free-molecule flow ($\lambda \gg D$), simple kinetic theory predicts[1] that

$$I(\phi) = I(0) \cos \phi, \tag{1}$$

where I(0) is the intensity along the center line ($\phi=0$). Our experimental results are in agreement with Eq. 1 only if the upstream pressure is sufficiently low to cause λ to be more than one order of magnitude greater than D. As the upstream pressure increases

*This work is supported by the National Aeronautics and Space Administration (Grant NsG-496).

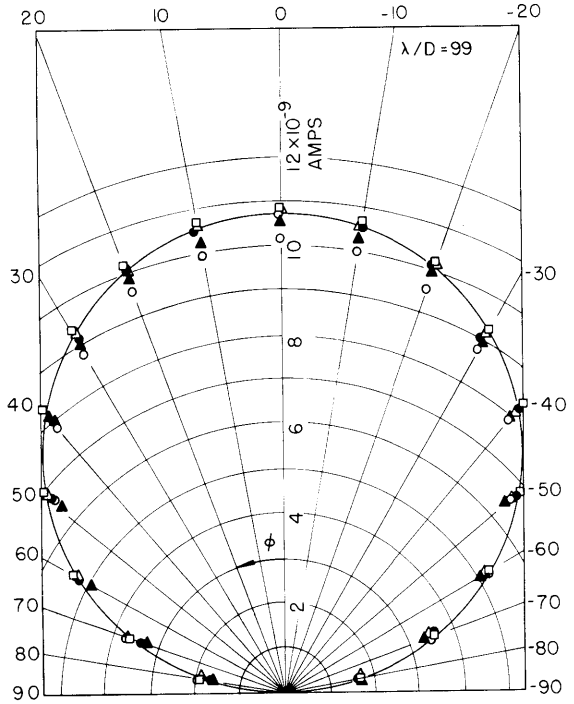

Fig. XII-6. Dependence of measured intensity on angular position from the center line of a sharp-edged orifice. Solid curve is the theoretical cosine distribution based on the corrected center-line intensity. Knudsen number, $\lambda/D = 99$.

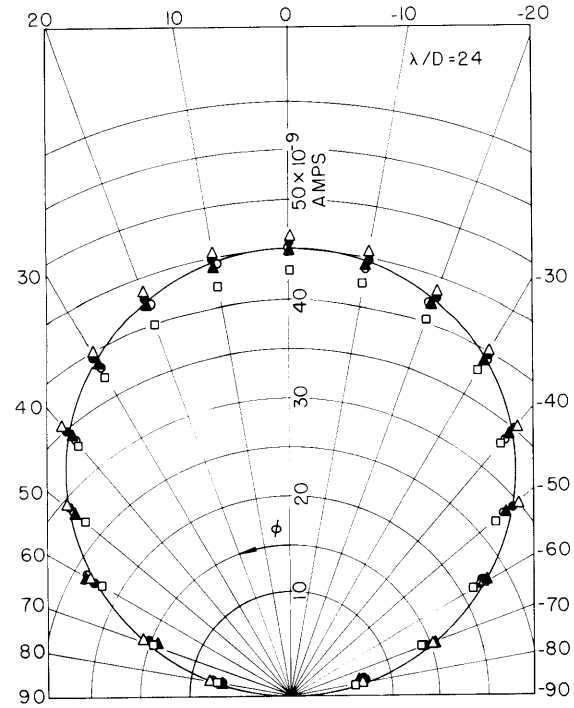

Fig. XII-7. Dependence of measured intensity on angular position from the center line of a sharp-edged orifice. Knudsen number, $\lambda/D = 24$.

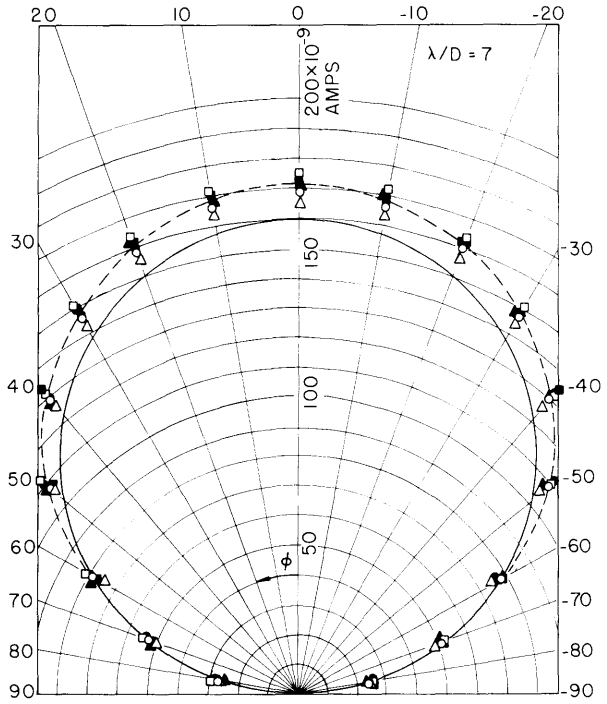

Fig. XII-8.

Dependence of measured intensity on angular position from the center line of a sharp-edged orifice. Knudsen number, $\lambda/D = 7$. Notice that the experimental data (dashed curve) deviate from the theoretical cosine distribution (solid curve).

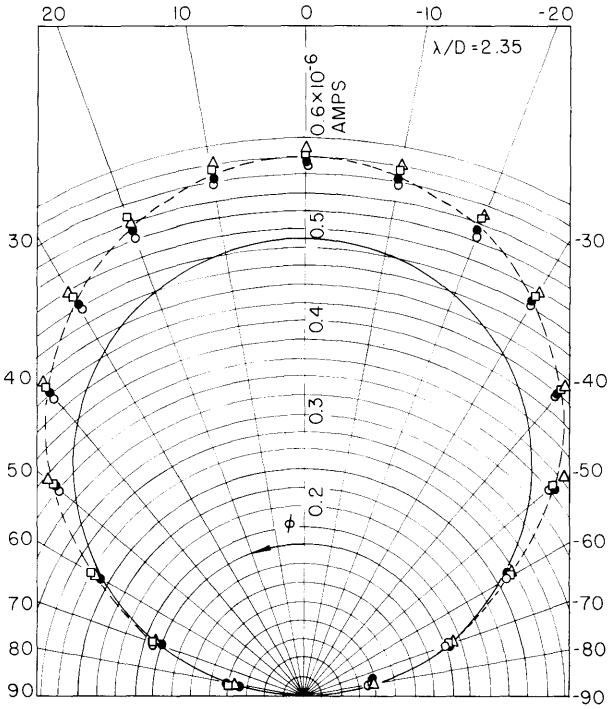

Fig. XII-9.

Dependence of measured intensity on angular position from the center line of a sharp-edged orifice. Knudsen number, $\lambda/D = 2.35$. Notice that the experimental data (dashed curve) deviate from the theoretical cosine distribution (solid curve).

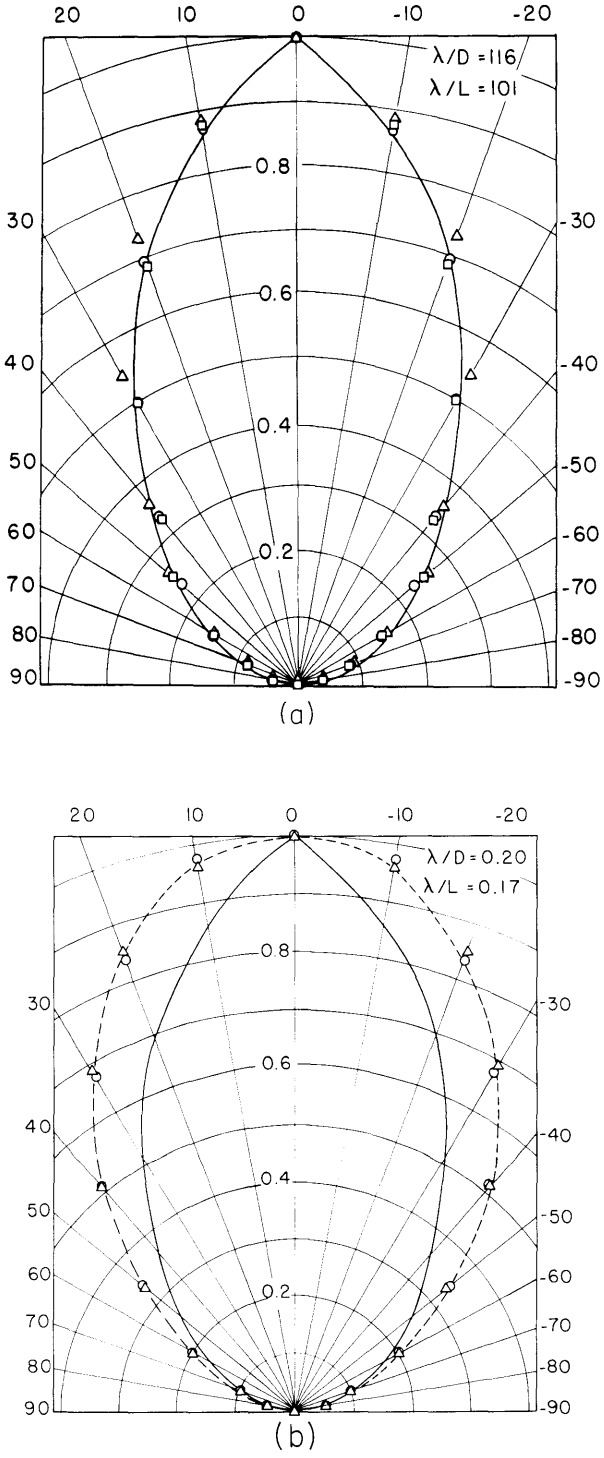

Fig. XII-10. Normalized intensity vs angle for flow from a tube having L/D = 1.15. (a) λ/D = 116. (b) λ/D = 0.20. Solid curve represents the theoretical prediction of Clausing (1930) for the free-molecule limit.

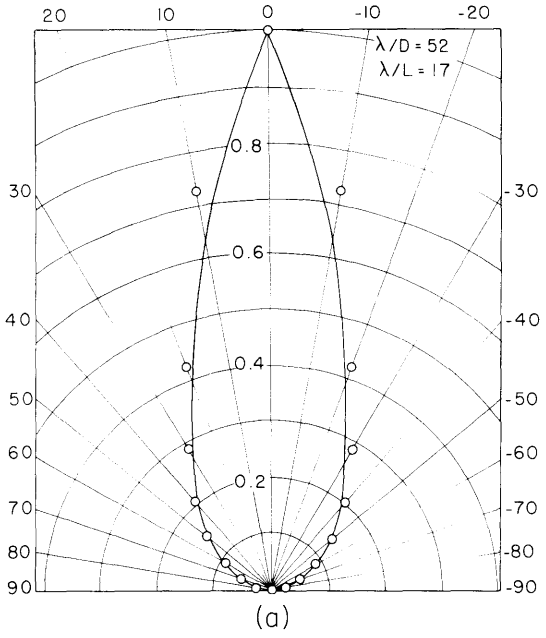

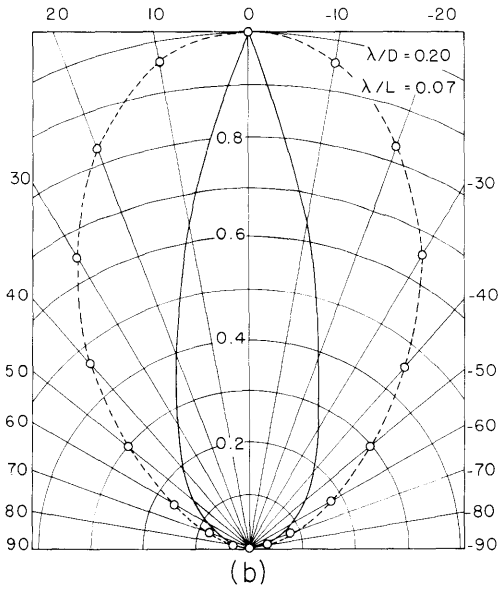

Fig. XII-11. Normalized intensity vs angle for flow from a tube having L/D = 3.03. (a) λ/D = 52. (b) λ/D = 0.20.

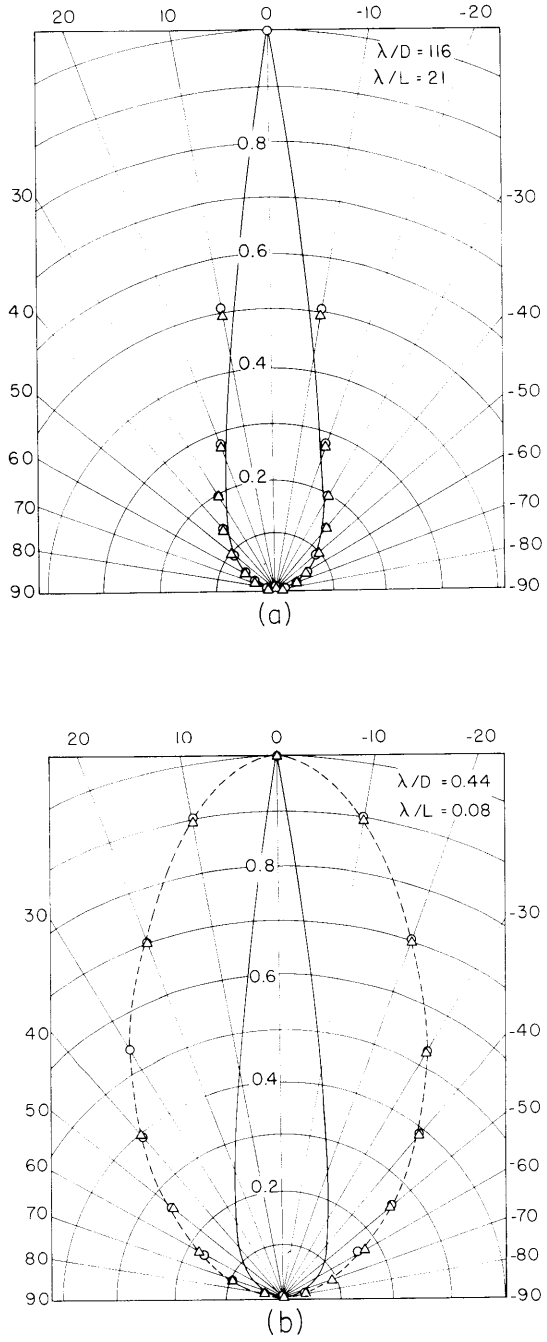

Fig. XII-12. Normalized intensity vs angle for flow from a tube having L/D = 5.63. (a) λ/D = 116. (b) λ/D = 0.44.

(that is, as λ decreases), the angular distribution deviates from the cosine relation because the intensity near the center line exceeds the free-molecule prediction. The data are shown in Figs. XII-6 through XII-9.

We have compared our measurements of the center-line intensity, I(0), with the theoretical predictions of Narasimha,[3] Willis,[4] and Morton.[5] These predictions have the following form in the near free-molecule flow regime:

$$I(0) = I(0)_{FM}\left[1 + A\frac{D}{\lambda}\right]. \tag{2}$$

$I(0)_{FM}$ is the limiting value for free-molecule flow as calculated by simple kinetic theory. The magnitude of A depends on the details of the theoretical treatment; Narasimha, Willis, and Morton obtain values of 0.30, 0.23, and 0.41, respectively. Our experimental data correlate best with A = 0.45.

The total mass flow rate may be calculated by integrating the measured angular distributions over the appropriate range of solid angles. These results are in agreement with the data reported by Liepmann.[6]

Tube Flow

Experiments similar to those described above were also performed for three cylindrical tubes having length-to-diameter ratios of 1.15, 3.03, and 5.63. The angular distributions are in general agreement with the analytical results of Clausing[7] when λ is much greater than both L and D. As observed for orifice flow, the angular distributions deviate from the free-molecule patterns as λ decreases. Typical results are shown in Figs. XII-10 through XII-12. The results for the center-line intensity, I(0), are particularly interesting for tube flow because they exhibit minima when plotted against D/λ. (See Fig. XII-13.) The minima become more pronounced with increasing

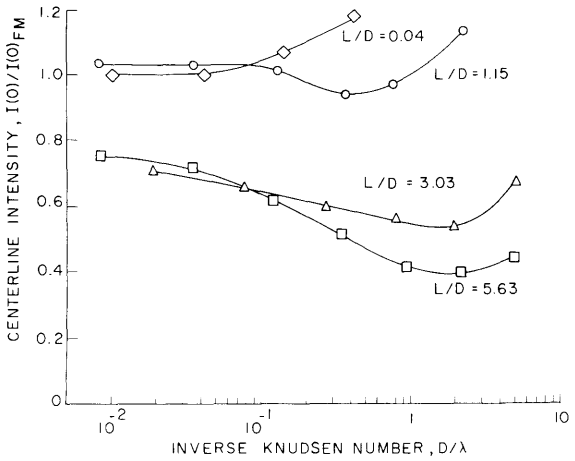

Fig. XII-13. Dependence of normalized center-line intensity on inverse Knudsen number for tubes of several length-to-diameter ratios.

L/D. Other investigators have observed a similar effect in the mass flow rate of gases through long capillary tubes. (Pollard and Present[8] have considered this problem in some detail.)

Present Work

Since existing theoretical treatments of near free-molecule flow through orifices and tubes do not satisfactorily describe our experimental results, we are continuing our attempts to obtain an analytical solution to the problem. The apparatus is now being modified so that we may proceed with measurements of the velocity distribution of the flow as a function of ϕ and λ/D.

R. E. Stickney

References

1. W. J. Hastings, S.M. Thesis, Department of Mechanical Engineering, M.I.T., 1964.
2. R. L. Keating, S.M. Thesis, Department of Mechanical Engineering, M.I.T., 1965.
3. R. Narasimha, J. Fluid Mech. 10, 371 (1961).
4. D. R. Willis, Aeronautical Engineering Report 683, Princeton University, March 1964.
5. H. S. Morton, Project Squid Technical Report UVA-4-P-1, University of Virginia, July 1964.
6. H. W. Liepmann, J. Fluid Mech. 10, 65 (1961).
7. P. Clausing, Z. Physik 66, 471 (1930); Ann. Physik 12, 961 (1932); also see B. B. Dayton, Am. Vacuum Soc. Trans., Vol. V, 1958.
8. W. G. Pollard and R. D. Present, Phys. Rev. 73, 762 (1948).

XII. PHYSICAL ELECTRONICS AND SURFACE PHYSICS

D. Neutralization of Space Charge in Thermionic Diodes*

Academic and Research Staff

Prof. R. E. Stickney

Graduate Students

A. G. F. Kniazzeh

RESEARCH OBJECTIVES

The performance of a thermionic energy converter depends strongly on the effectiveness of the technique used to neutralize the electron space charge. The three common techniques for generating the ions required for neutralization are (i) surface ionization at the emitter, (ii) ionization within the plasma by various electron, photon, or atom impact processes, and (iii) auxiliary sources. We are investigating the physical processes and relative merits of each of these techniques.

R. E. Stickney

1. CESIUM MOLECULAR-ION FORMATION BY COLLISION OF TWO EXCITED ATOMS II

Models proposed to explain the voltage-current curves of cesium thermionic diodes operating in the ignited mode have generally incorporated three volume ionization mechanisms: by electron impact with ground-state cesium atoms; by electron impact with cesium atoms in the first excited state; and cesium molecular-ion formation by the collision of two excited atoms[1-3] according to the process

$$2Cs(6p) \rightarrow Cs_2^* \rightarrow Cs_2^+ + e. \qquad (1)$$

By using Warner's[4] calculation with measured[5,6] and calculated[7] cross sections, ionization by the first two mechanisms can be shown to be deficient for sheath neutralization by a factor of 10 for some experimentally observed diode conditions. On the other hand, Witting and Gyftopoulos[2] have calculated a molecular-ionization cross section that makes ionization according to Eq. 1 very attractive.

This report concerns an optical pumping experiment similar to Freudenberg's,[8] by which an upper bound is established for σ_m, the cross section for molecular-ion production by process (1).

---

*This work is supported by the Joint Services Electronics Programs (U.S. Army, U.S. Navy, and U.S. Air Force) under Contract DA 36-039-AMC-03200(E).

a. Description of the Experiment

In our experiment, a cylindrical resonance tube containing cesium is irradiated by resonance radiation of λ8521 Å coming through an interference filter from a cesium arc lamp, as shown in Fig. XII-14. The radiation is absorbed in the cesium, thereby producing atoms in the first excited state which collide and produce molecular ions by process (1). The ions formed within the volume enclosed by the dashed lines in Fig. XII-14

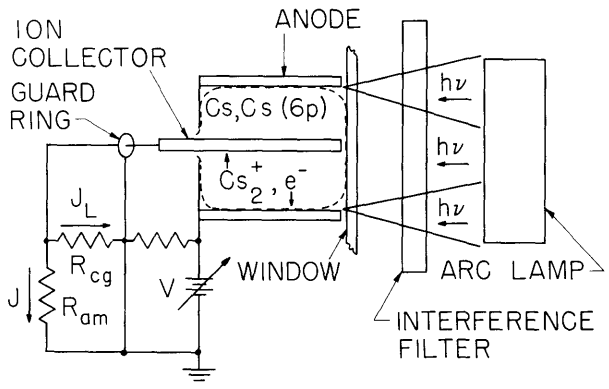

Fig. XII-14. Optical pumping arrangement.

are drawn to an axial collector by an applied potential V, and the difference in the values of this collector current measured when the arc irradiates the absorption tube and when the arc radiation is blocked is used to calculate the cross section.

Many radiation-dependent currents might be included in this difference current, so, in general, the difference current J will consist of the following terms:

$$J(R_{cg}+R_{am})/R_{cg} = J_m - J_r - J_{an} + J_\nu + \text{negligible positive terms.} \quad (2)$$

Here,

R_{cg} is the leakage resistance from the ion collector to the guard ring (≈1 MΩ),

R_{am} is the input impedance of the electrometer in the feedback mode (≈0.15 MΩ),

J_m is the total amount of charge produced per unit time by molecular-ion formation by process (1),

J_r is the current associated with the molecular ions that recombine before being collected,

J_{an} is the molecular-ion current that is collected on the window or anode, and

J_ν is the photoelectric current from the ion collector produced by the arc radiation.

J_r is negligible because of the small size of J($\sim 10^{-10}$ amp), and at 6 volts applied voltage J_{an} is less than 20 per cent of J_m for the conditions of the experiment. Thus, to a

good approximation

$$\frac{R_{cg} + R_{am}}{R_{cg}} J \approx J_m + J_\nu, \tag{3}$$

and certainly

$$J_m \leq 1.25 \frac{R_{cg} + R_{am}}{R_{cg}} J. \tag{4}$$

Even though the resonance chamber is irradiated by radiation that is resonant with the $6p_{3/2}$ state, we must also consider ionizing collisions involving $6p_{1/2}$ atoms that are formed by quenching collisions of $6p_{3/2}$ atoms with ground-state atoms according to the process

$$Cs(6p_{3/2}) + Cs(6s) \longleftrightarrow Cs(6p_{1/2}) + Cs(6s) + 0.068 \text{ ev}. \tag{5}$$

Then J_m will consist of a sum of terms corresponding to collisions of two 6p atoms with various j values:

$$J_m = \frac{e\bar{v}}{\sqrt{2}} \left(\sigma_{m11} \int d^3r N_1^2 + \sigma_{m12} \int d^3r 2N_1N_2 + \sigma_{m22} \int d^3r N_2^2 \right). \tag{6}$$

Here,

e is the electronic charge,

$\bar{v}$ is the average thermal velocity of the atoms,

the integral is over the volume of the resonance chamber,

N_1 is the density of $6p_{3/2}$ excited atoms,

N_2 is the density of $6p_{1/2}$ excited atoms, and

σ_{mij} are the cross sections at 500°K for the production of molecular ions by the collision of excited atoms of types i and j.

The excited atom densities are determined by two radiation transport equations that are solved to give estimates of the integrals appearing in (6). The resulting integral of N_2^2 is less than the other two integrals because quenching is not efficient enough to produce a large $Cs(6p_{1/2})$ density for our experimental conditions. Since the electronic energy of two $6p_{1/2}$ atoms is $0.09 \pm .05$ ev below the energy required to form a cesium molecular ion, we can also assume that σ_{m22} is less than σ_{m11} or σ_{m12} so that the last term of (6) can be neglected. Furthermore, for our experimental conditions $\int d^3r N_1^2$ is within a factor of 2 of $\int d^3r 2N_1N_2$ so that, no matter what the ratio of σ_{m11} to σ_{m12}, we can approximate to 33 per cent.

$$\sigma_{m11} \int d^3r N_1^2 + \sigma_{m12} \int d^3r 2N_1N_2 \approx \sigma_m \int d^3r N_1(N_1+2N_2), \tag{7}$$

where σ_m is the effective molecular-ionization cross section,

$$\sigma_m = (\sigma_{m11}+\sigma_{m12})/2. \tag{8}$$

Then J_m is given by

$$J_m = \frac{e\bar{v}}{\sqrt{2}}\sigma_m \int d^3r N_1(N_1+2N_2). \tag{9}$$

The order of magnitude of J_ν can be estimated by measuring J_W, the ion-collector current produced by shining a standard tungsten lamp (operating at 15 amps) through the interference filter and onto the collector of the resonance tube. Then if F and $F_W = 1.6 \times 10^3$ erg/sec are the calculated radiant-energy fluxes to the ion collector from the arc and tungsten lamps, respectively, we have

$$J_\nu = C\frac{F}{F_W} J_W \left(\frac{R_{cg} + R_{am}}{R_{cg}}\right), \tag{10}$$

where C (of order unity) is an approximate correction factor accounting for variations in the photoelectric quantum yield over the ion-collector surface.

Combining (3), (9), and (10) gives

$$J = \frac{e\bar{v}}{\sqrt{2}}\sigma_m \frac{R_{cg}}{R_{am}+R_{cg}} \int d^3r N_1(N_1+2N_2) + C\frac{F}{F_W} J_W. \tag{11}$$

We shall determine the constants σ_m and C by correlating measured values of J, J_W, and R_{cg} and calculated values of N_1, N_2, F, and F_W. Since the resulting effective cross section is small, we then return to (4) to determine the upper bound to σ_m.

The essential requirement of this argument is to demonstrate the validity of the excited-atom density distributions used in the calculation. This is accomplished by a description of the experimental apparatus followed by a discussion of the radiation transport equations that determine the excited-atom density under various experimental conditions.

b. Experimental Apparatus

The main components of the experimental apparatus are shown in Fig. XII-15. Not shown are power supplies, arc heaters, 17 thermocouples, and an electrometer and recorder that measure the ion-collector current. The temperature of the cesium in the resonance chamber was set at approximately 500°K throughout the experiment and was controlled by the front heater which also heated the front window. In order to insure that a cesium film would not form on the front window, extra heater windings were placed on the front face of the front heater. Also, the front heater was placed against the

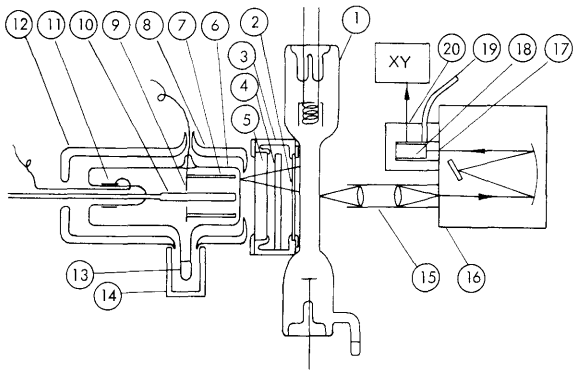

1.	QUARTZ-CESIUM ARC LAMP	11.	COLLECTOR GUARD RING
2.	PYREX WINDOW	12.	BACK HEATER
3.	FAN CHANNEL	13.	CESIUM RESERVOIR
4.	ABSORPTION FILTER	14.	CESIUM HEATER
5.	INTERFERENCE FILTER	15.	ENCLOSED INPUT OPTICS
6.	CESIUM RESONANCE TUBE	16.	CALIBRATED SPECTROMETER
7.	POLISHED OFHC-Cu ANODE	17.	HEATED PYREX WINDOW
8.	FRONT HEATER	18.	RCA 7102 PHOTOMULTIPLIER
9.	STAINLESS ABSORBING PLATE	19.	DRY NITROGEN
10.	POLISHED Cu ION COLLECTOR	20.	DRY ICE AND ACETONE

Fig. XII-15. Experimental apparatus.

housing of the interference filter to limit convection cooling of the window, and the reflecting side of the filter was faced toward the window to reduce radiation cooling.

The resonance tube was assembled, under a reducing gas atmosphere to inhibit oxidation of the electrodes, and then baked on an oil diffusion pump at 380°C for 3 days to a final pressure of 2×10^{-6} torr. A cesium ampoule was then attached, and the tube was baked for 2 days at 180°C to a pressure of 10^{-6} torr. Finally, the ampoule was broken, the cesium was vacuum-distilled into the appendage, and the tube was sealed off.

The arc lamp operated at 0.1-0.35 torr cesium pressure, 13-17 volts, and 25-50 amps. Quartz was used for the arc envelope, because of serious melting problems encountered with Pyrex. Cesium attack of the quartz produced an absorbing and partially reflecting dielectric film on the center section of the arc envelope which deteriorated arc performance with use. There were also short-term fluctuations of the arc intensity caused by relaxation of the various temperatures in the arc following a step in arc current. Since the excited-atom density in the resonance tube was proportional to the incident radiation intensity, the intensity of the arc at the center of the $\lambda 8521$ Å line was monitored continuously by using a calibrated Jarrell-Ash 500-mm spectrometer and an RCA 7102 photomultiplier. Occasionally, arc line shapes were recorded also. The $\lambda 8521$ Å line shapes obtained experimentally showed no shifts outside the uncertainty in the spectrometer frequency calibration (0.15 Å), and no self-absorption for pressures below ~0.25 torr and currents above ~30 amps. On the contrary, the arc line shapes

at high current and low pressure were quite peaked, and did not exhibit a flat portion that is characteristic of a spatially uniform excitation temperature. The intensity at line center corresponded to an excitation temperature of between 2500°K and 3500°K. The optical system used for arc-intensity measurements was calibrated in frequency by using a small mercury lamp, and in intensity by using a secondary standard tungsten lamp.

Calculations[9] show that spectrometer broadening did not affect the line shapes by more than 15 per cent.

Since the experiment requires a large primary radiation intensity, it was necessary to keep the optical path from the arc to the absorption tube as short as possible. With this geometry and with the absorbing side of the interference filter facing the arc, it was necessary to cool the filter by placing it in a fan duct. The temperature of the filter varied from 70° to 110°C during a run; however, this high temperature did not affect its transmission properties permanently. The blocked filter had a maximum transmission of 0.65 with half-transmission points at 90°C at approximately λ8430 Å and λ8635 Å, and less than 0.001 transmission outside the range λ8280 Å-λ8750 Å.

Data were taken with the arc operating at various pressures and currents and with the absorption-tube cesium pressure and ion-collector temperature set at various levels. The bias voltage (V, in Fig. XII-15) was usually set at 6 volts, since this was found sufficient to saturate the current, J. For each setting of the arc and absorption-tube conditions, measurements of the ionization current were taken on an electrometer and a time-running XY recorder, while various absorption filters were inserted in the fan duct to attenuate the primary radiation. An average of 7 data points was taken for each set of conditions.

c. Analysis

The excited-atom densities are determined by two coupled radiation transport equations which account for the absorption and re-emission of resonance radiation and the de-excitation of excited atoms by quenching collisions with ground-state atoms. The rigorous derivation of the radiation transport equations is lengthy and can be found elsewhere.[10] As a first approximation, we neglect excited-atom diffusion[11]; assume that the polished copper anode and ion collector are specularly reflecting,[12] the stainless-steel plate (9, in Fig. XII-15) is perfectly absorbing, and the front window is transmitting to scattered photons; approximate the arc lamp as spatially uniform in intensity and as filling the small solid angle of acceptance of the interference filter for λ8521 Å radiation (as shown by the cones of acceptance of Figs. XII-14 and XII-15). Then the problem becomes one of radiation transport in plane-parallel layers[13] in which the spatial variation of the excited-atom density depends only on the distance y into the resonance tube measured from the front window.

We also assume that scattering of radiation is isotropic in direction and incoherent

in frequency. These last two approximation lead to a form of the Holstein-Biberman[14] transport theory which is appropriate to quenching.[15]

Taking account of hyperfine structure[16] and Doppler, natural,[17] and resonance broadening,[18] we find that a transmission function $L_i(y)$ can be approximated to ±20 per cent over more than 98 per cent of the resonance chamber[2,14,15] by

$$L_i(y) = \left[\int d\nu\, k_i(\nu) \exp[-k_i(\nu)y]\right]\left[\int d\nu\, k_i(\nu)\right]^{-1} = 1.15(\pi k_{p1} y)^{-1/2}, \tag{12}$$

where $k_i(\nu)$ is the absorption coefficient for radiation of frequency ν near ν_{oi}, the unperturbed frequency for the $6p_i$-6s transition; and k_{p1} is the absorption coefficient at line center for the resonance-broadened $6p_{3/2}$-6s line without hyperfine structure. We also calculate the amount of radiation absorbed per unit volume from the primary arc intensity. For this calculation, we approximate the typical arc line shape, shown as the curved line in Fig. XII-16a, by a triangle. The height of the triangle is determined by I_o, the average intensity at the wavelengths of the two effective hfs components of the $6p_{3/2}$-6s line. The width of the triangle $\Delta\lambda_A$ is determined by the full width of the true arc line at an intensity equal to one-half I_o, as shown in Fig. XII-16a. Using this triangular approximation and detailed balance,[18] we calculate the normalized arc transmission H(x, z) shown in Fig. XII-16b. Here x is the normalized optical depth, calculated by using Gregory's resonance-broadening data and oscillator strengths[18,19] which satisfy the sum rule, and z is the normalized arc linewidth:

$$x = \frac{k_{p1} y}{2}\left[\frac{\Delta\lambda_{p1}}{\Delta\lambda_{hfs,1}}\right]^2 = 3.2 \times 10^4 p_o^2 \frac{y}{y_o}; \qquad x_o(p_o) \equiv x(y=y_o) \tag{13a}$$

$$z = \frac{\Delta\lambda_A}{\Delta\lambda_{hfs,1}} > 3.9. \tag{13b}$$

Here $\Delta\lambda_{hfs,1}$ is the effective hfs splitting, $\Delta\lambda_{p1}$ is the full half-width for resonance broadening of the $6p_{3/2}$-6s line, p_o is the reduced pressure in torr, and y_o is the depth of the resonance chamber.

The quenching frequencies associated with (5) and with quenching to the ground state are calculated from the results of resonance-fluorescence experiments[20,21] and arc power measurements.[22] The neglect of quenching by contaminants[23,24] is justified if the pressure of contaminants is below 3×10^{-3} torr.

The preceding approximations result in two coupled, singular, integral, radiation transport equations whose approximate solutions are

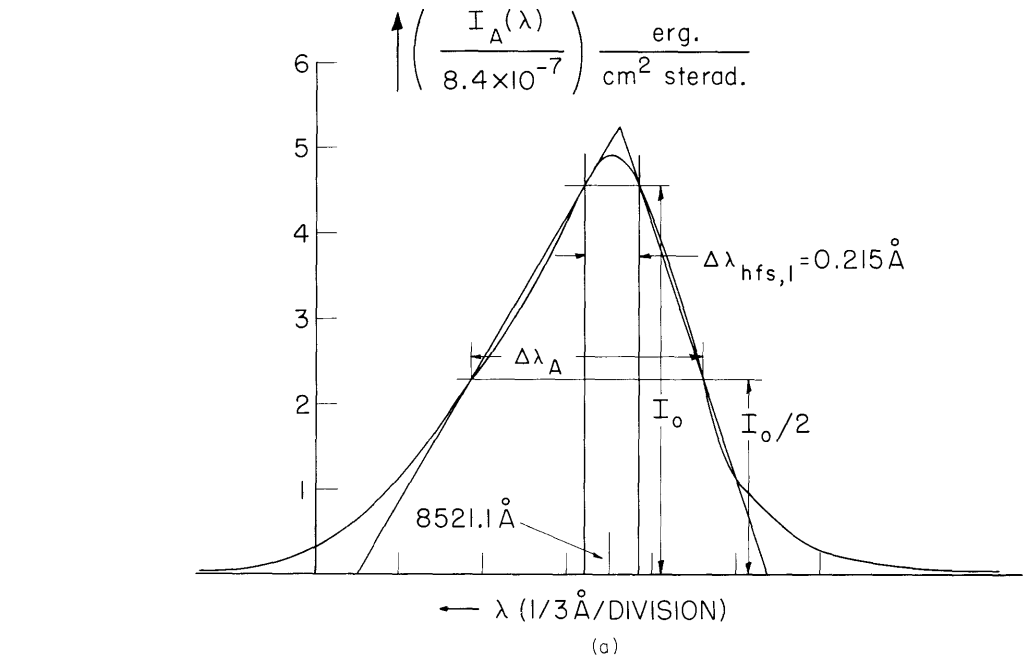

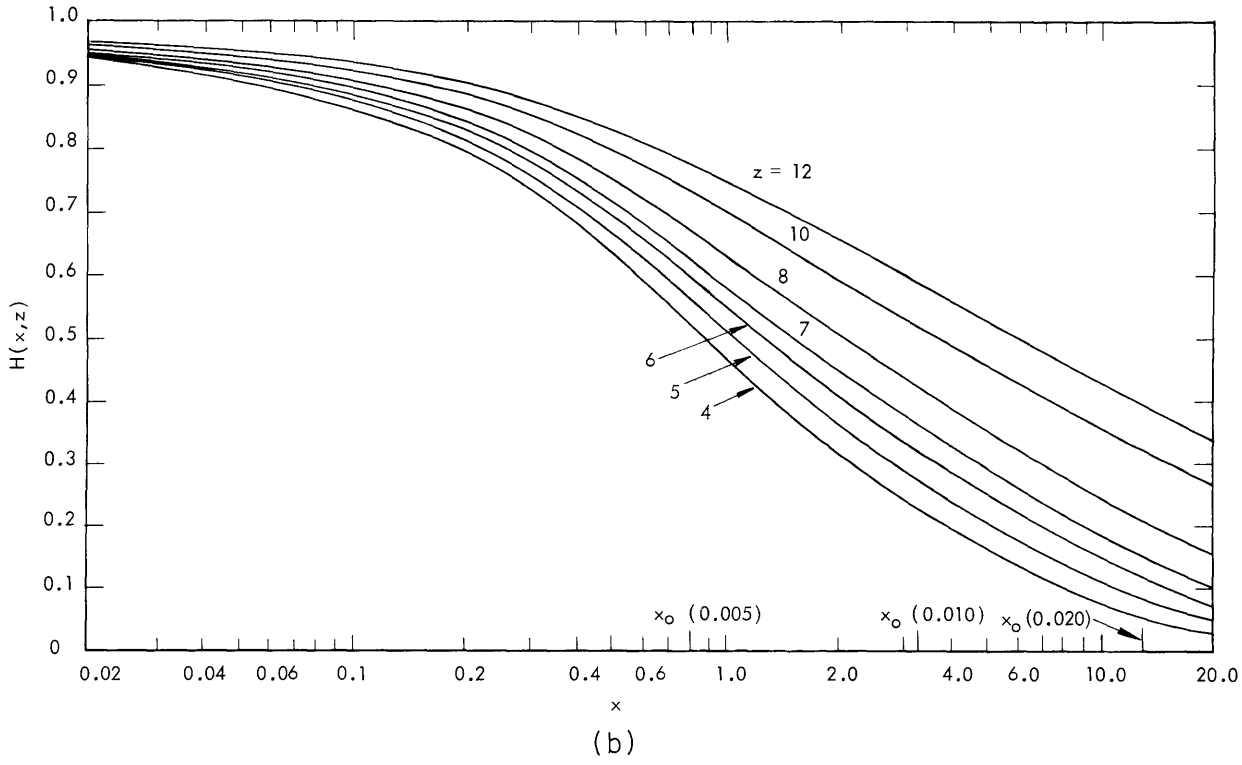

Fig. XII-16. (a) Arc line shape (40 amps, 0.15 torr).
(b) Normalized arc transition, H(x, z).

$$n_1(x) = \frac{\left[0.66 + x^{-1/2} + (x_o - x)^{-1/2}\right] H(x,z)}{\left[2.16 + x^{-1/2} + (x_o - x)^{-1/2}\right]\left[1 + \left(\frac{x}{x_o - x}\right)^{1/2}\right]} \tag{14a}$$

$$n_2(x) = \frac{1.50 H(x,z)}{\left[2.16 + x^{-1/2} + (x_o - x)^{-1/2}\right]\left[1 + \left(\frac{x}{x_o - x}\right)^{1/2}\right]} \tag{14b}$$

where

$$n_i = \frac{2}{3\bar{t}} \cdot \frac{2h\nu_{o1}}{\lambda_{o1}^2 I_o} \cdot \frac{g_1 N_i}{g_o N_o}, \tag{15}$$

h is Planck's constant, ν_{o1} and λ_{o1} are the frequency and wavelength of the $6p_{3/2}$-6s line, $g_o = 2$ and $g_1 = 4$ are the statistical weights of the 6s and $6p_{3/2}$ states, N_o is

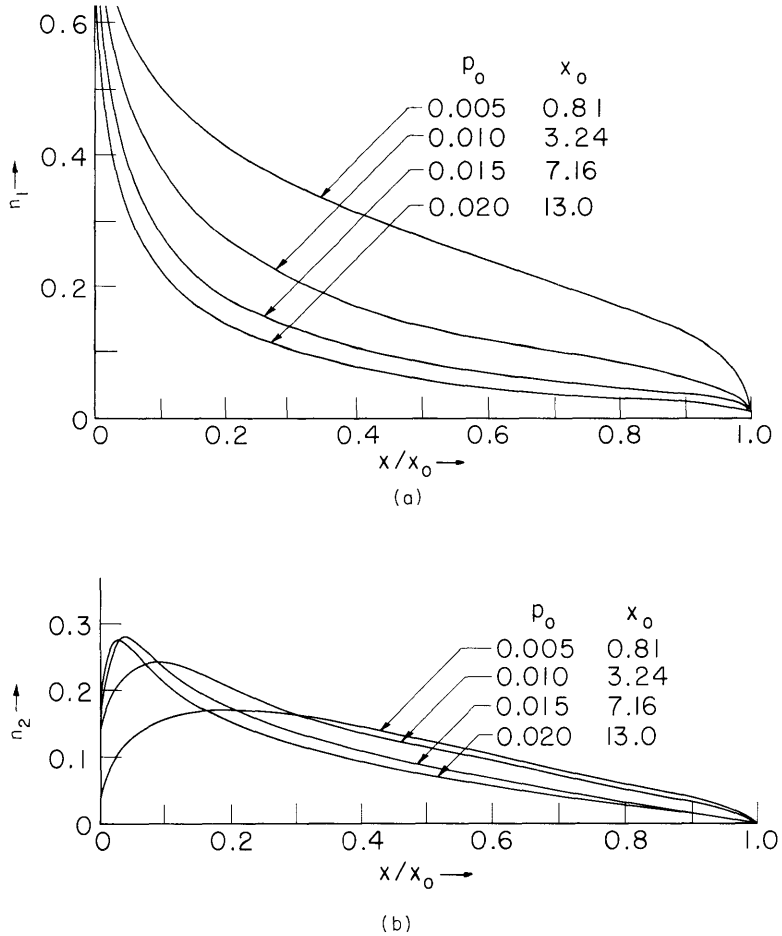

Fig. XII-17.

(a) $n_1(x)$ for z = 4.2.

(b) $n_2(x)$ for z = 4.2.

the Cs(6s) density, and $\bar{t}$ is the average of $t'(\theta)$, the transmission of the interference filter and two layers of Pyrex for λ8521 Å radiation incident at an angle θ,

$$\bar{t} = \int_0^{\pi/2} t'(\theta) \sin\theta \, d\theta = .018. \tag{16}$$

The excited-atom densities given by (14) are plotted in Fig. XII-17 for typical conditions.

Finally, the total charge production rate by process (1) is given by Eqs. 9 and 15:

$$J_m = \frac{10^{-5} e\bar{v}}{\sqrt{2}} \left[\frac{3\lambda_{01}^2 \bar{t} I_o g_1 N_o}{4h\nu_{01} g_o p_o}\right]^2 \pi R^2 y_o \sigma_m \Phi, \tag{17}$$

where R = 0.95 cm and y_o = 2.5 cm are the radius and length of the resonance chamber, and

$$\Phi = 10^5 p_o^2 \int_0^{x_o} n_1(n_1+2n_2) \frac{dx}{x_o}. \tag{18}$$

Φ is calculated numerically from Eq. 14 and is plotted in Fig. XII-18. We also use (14) and (15) to find the contribution to F from scattered λ8521 Å radiation.

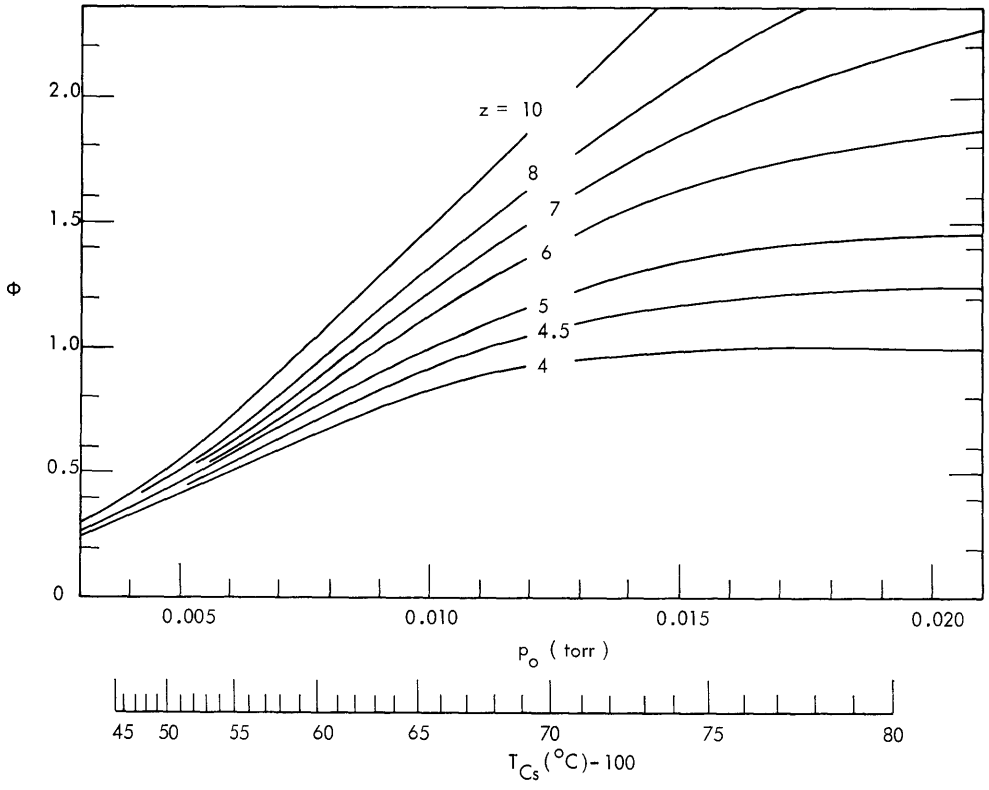

Fig. XII-18. Normalized excited-atom density integral.

Using this calculated F and (17) in (11) and evaluating the known quantities yields the correlation equation

$$J/A = \sigma_m + C\Psi \quad (\mathring{A}^2) \,, \tag{19}$$

where

$$A = 200 I_o^2 \Psi R_{cg}(R_{cg}+R_{am})^{-1} \quad (\text{amp}/\mathring{A}^2) \tag{20}$$

$$\Psi = 10^5\left[z+133p_o^{1/2}\right] I_o J_W/A \quad (\mathring{A}^2) \,. \tag{21}$$

Here, I_o is in erg/cm^2 steradian, J and J_W are in amps, and p_o is in torr.

d. Results and Conclusion

Data were taken for a resonance chamber temperature of 500°K, for various bias voltages V (usually 6 volts), and for various values of the resonance tube cesium-reservoir temperature T_{Cs}, the ion-collector temperature T_c, the arc cesium-reservoir temperature T_A, and the arc current J_A. Also, various absorption filters f_i were inserted in the fan channel of Fig. XII-15 to attenuate the arc intensity. The resulting ion-collector currents $J(f_i)$ were correlated with $t(f_i)I_o$, replacing I_o in Eqs. 20 and 21, where $t(f_i)$ is the transmission of f_i at λ8521 Å:

$$t(f) = 0.53, \qquad t(f_1) = 0.19, \qquad t(f_2) = 0.70. \tag{22}$$

R_{cg} and J_W were found to depend almost exclusively on the variable

$$\tau = 1000/T_{Cs} - 1000/T_c. \tag{23}$$

J_W was found to saturate at ~0.5 volt and to depend linearly on the tungsten lamp intensity, thereby clearly indicating its photoelectric origin. J and I_o were measured simultaneously during a run; J_W, R_{cg}, and z were measured between J-runs or were determined by interpolation, with the use of correlations of $J_W(\tau)$, $R_{cg}(\tau)$ and $z(T_A, J_A)$ and measured values of τ, T_A, and J_A. The ranges of the experimental variables appearing in (19) are listed in Table XII-2.

The correlation of these data as presented in Fig. XII-19 is best described by the relation

$$J/A = \left(0.07 \,{}^{+.04}_{-.03}\right) + (0.1 \pm .05)\,\Psi \quad (\mathring{A}^2). \tag{24}$$

Since the uncertainty in the values of I_o and J_W and the approximations made in the analysis probably introduce errors of less than a factor of 2, the effective cross section

Table XII-2. Ranges of variables entering into Eq. 14.

J, J(f), $J(f_1)$ (10^{-10} amp)	.2-2.5	τ	.16-.33
	.1-1.0	J_W (10^{-10} amp)	.12-3.9
	.02-.22	R_{cg} (10^6 ohm)	.4-7.8
T_{Cs} (°C)	143-182	I_o(10^{-6} erg/cm^2)	1.2-4.0
T_c (°C)	183-230	z	3.9-15.4
J_A (amp)	20-50	Φ	.26-1.94
T_A (°C)	207-257	A (10^{-10} amp/Å^2)	1.4-20.9

indicated by (24) is within a factor of 3 of

$$\sigma_m = 0.07\ \text{Å}^2. \tag{25}$$

This interpretation of the data is supported by the intensity dependence of J plotted in Fig. XII-20. Except for the points that have tails to the right, fall higher than the rest, and correspond to conditions for which the arc line shapes are self-absorbed, the ratio $J(f_i)/J$ is close to $[t(f_i)]^2$ at low Ψ, and approaches $t(f_i)$ at large Ψ. This indicates that a large part of J at low Ψ is due to molecular ions, while J_ν dominates at large Ψ. (Here, Ψ is calculated with the unattenuated intensity I_o, not with $t(f_i)I_o$.) Also shown are curves of $J(f_i)/J$ calculated by using Eq. 24 with $\sigma_m/C = 0.7\ \text{Å}^2$ and $2.2\ \text{Å}^2$:

$$\frac{J(f_i)}{J} = \frac{f_i\sigma_m/C + \Psi}{\sigma_m/C + \Psi} f_i. \tag{26}$$

These curves fall among the data points, thereby indicating that σ_m/C of Eq. 14 has the right order of magnitude.

An alternative interpretation of the data might be that all of the observed ion-collector current is due to photoelectric emission, as indicated by the straight line in Fig. XII-19. This interpretation, however, does not describe the trends of either Fig. XII-19 or Fig. XII-20. Whichever interpretation is accepted, the upper bound to σ_m is still given by

$$\sigma_m < 0.2\ \text{Å}^2. \tag{27}$$

If we disregard a factor of 1.25, this is the result that would be obtained by applying (14) to the data of Fig. XII-19 for low Ψ.

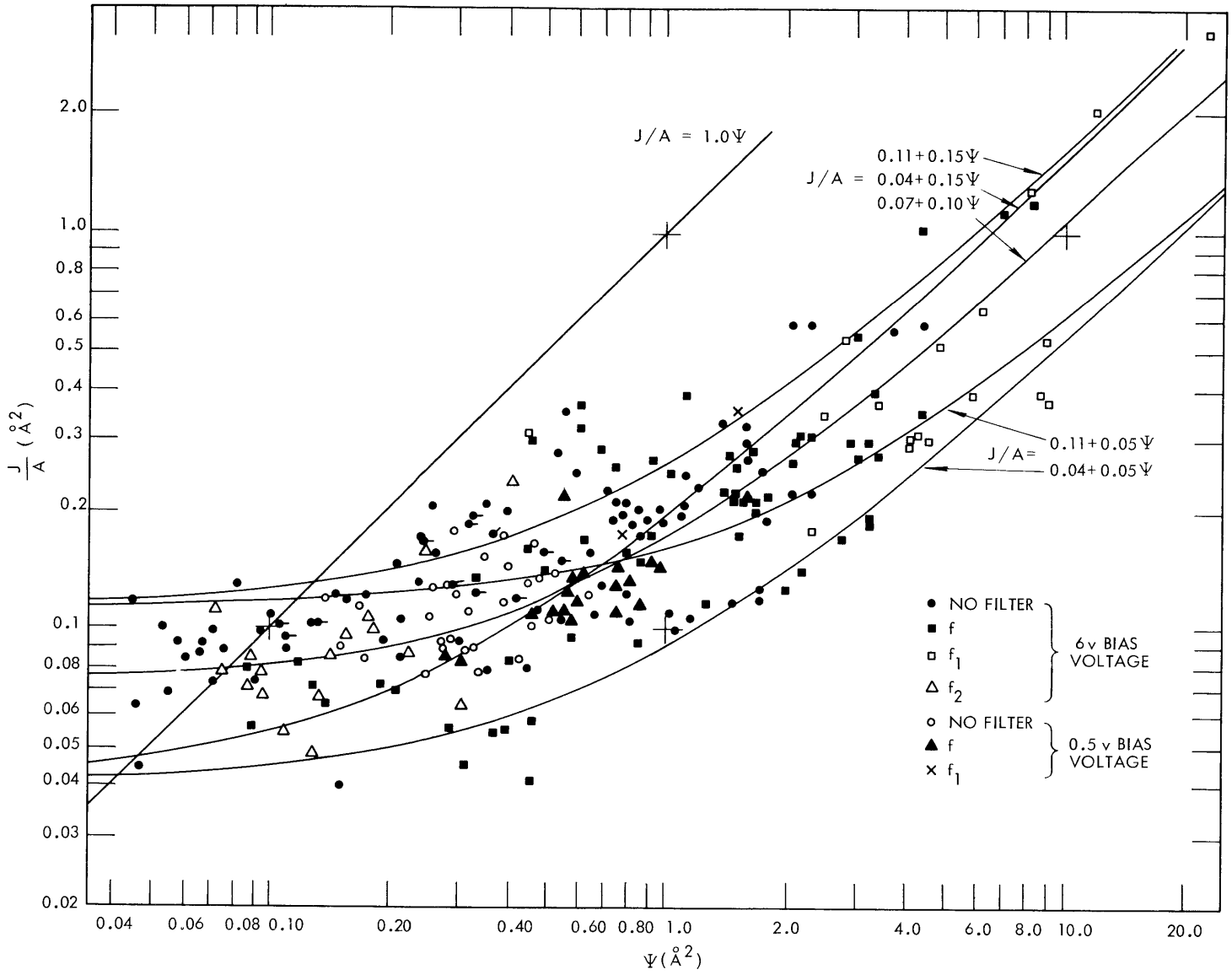

Fig. XII-19. Correlation of collector-current data.

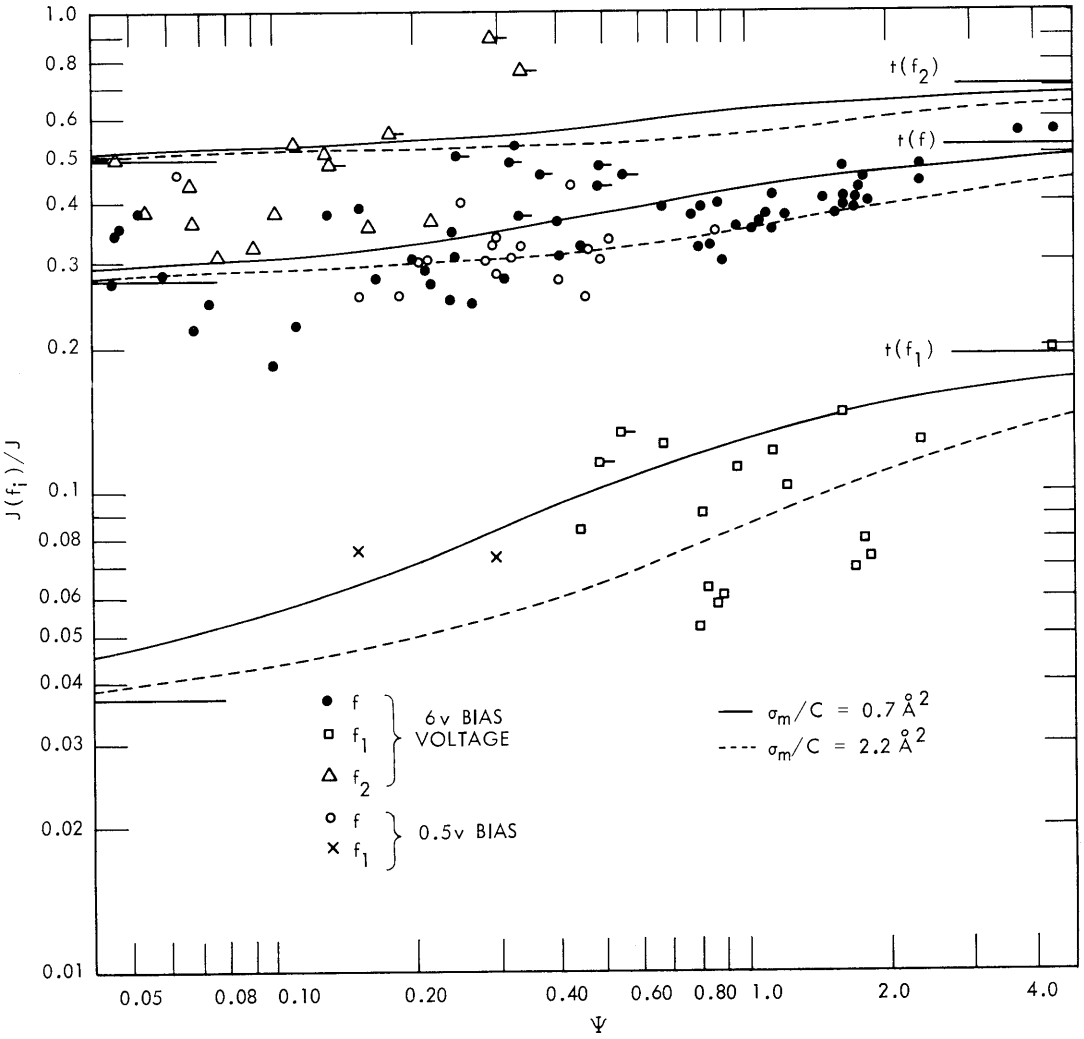

Fig. XII-20. Intensity dependence of the ion-collector current.

Table XII-3. Comparison of cross-section estimates for process (1).

Condition	Requirement	T(°K)
This experiment	$\sigma_m < 0.2$ Å^2	500
Harris[25] (Hammer and Aubrey[26]) recombination data used with Witting and Gyftopoulos[2] calculation	$\sigma_m < 7$ Å^2 ($\sigma_m < 18 \pm 13$ Å^2)	1600 (1380)
Cs_2^+ production dominates Cs^+ production from 6s and 6p states (following Warner[4-7])	$\sigma_m > 2.1$ Å^2	1600
Cs_2^+ ions neutralize the electrode sheaths[4]	$\sigma_m > 20$ Å^2	1600

Comparison of this result with other entries in Table XII-3 shows that if the cross section is not a strong function of temperature, molecular-ion production by the collision of two 6p cesium atoms will neither dominate ionization from the 6s and 6p states, nor, a fortiori, provide sufficient ions to neutralize the electrode sheaths in a cesium thermionic diode.

A. G. F. Kniazzeh

References

1. E. N. Carabateas and A. G. F. Kniazzeh, Proc. Thermionic Conversion Specialist Conference, Gatlinburg, Tennessee, October 1963, p. 63.
2. H. L. Witting and E. P. Gyftopoulos, J. Appl. Phys. 36, 1328 (1965).
3. D. H. Pollack and A. O. Jensen, J. Appl. Phys. 36, 3184 (1965).
4. C. Warner, Report on Twenty-fifth Annual Physical Electronics Conference, Massachusetts Institute of Technology, March 24-26, 1965, pp. 29-37.
5. R. H. McFarland and J. D. Smith, Phys. Rev. 137, A1058 (1965).
6. J. T. Tate and P. T. Smith, Phys. Rev. 46, 773 (1934).
7. J. W. Sheldon and J. V. Dugan, J. Appl. Phys. 36, 650 (1965).
8. K. Freudenberg, Z. Physik 67, 417 (1939).
9. A. G. Emslie and G. W. King, J. Opt. Soc. Am. 43, 658 (1955).
10. A. G. F. Kniazzeh and E. N. Carabateas, a paper presented at the Thermionic Conversion Specialist Conference, San Diego, California, October 1965.
11. T. Watanabe, Phys. Rev. 138, A1573 (1965); 139, AB1 (1965); 140, AB5 (1965).
12. S. Roberts, Phys. Rev. 118, 1509 (1960).
13. V. V. Sobolev, A Treatise on Radiative Transfer (D. Van Nostrand Company, New York, 1963).
14. T. Holstein, Phys. Rev. 72, 1219 (1947); 81, 1159 (1951).
15. R. Seiwert, Ann. Physik 18, 35 (1956); 17, 371 (1956).
16. H. Kopfermann, Nuclear Moments (Academic Press, New York, 1958).
17. A. C. G. Mitchell and M. W. Zemanski, Resonance Radiation and Excited Atoms (Cambridge University Press, London 1961), Chapter III.
18. G. P. Reck, H. Takebe, and C. A. Mead, Phys. Rev. 137, A683 (1965).
19. C. Gregory, Phys. Rev. 61, 465 (1942).
20. M. Czajkowski and L. Krause, Can. J. Phys. 43, 1259 (1965).
21. H. Bunke and R. Seiwert, Opt. Spectr. Aller Wellenlangen (Academie Verlag, Berlin, 1962).
22. F. L. Mohler, J. Res. Natl. Bur. Std. (U.S.) 9, 25 (1932).
23. R. G. W. Norrish and W. MacF. Smith, Proc. Roy. Soc. (London) A176, 205 (1940).
24. J. A. Jordan, Jr., and P. A. Franken, Phys. Rev (accepted for publication).
25. L. P. Harris, J. Appl. Phys. 36, 1543 (1965).
26. J. M. Hammer and B. B. Aubrey, Phys. Rev. (accepted for publication).